RSC Advances

PAPER

View Article Online
View Journal | View Issue

Cite this: *RSC Adv.*, 2020, **10**, 36111

HKUST-1 derived Cu@CuO_x/carbon catalyst for base-free aerobic oxidative coupling of benzophenone imine: high catalytic efficiency and excellent regeneration performance†

Huang Kaimeng,[a] Chen Siyuan,[b] Xia Changjiu,[a] Li Chenhao,[a] Zhu Bin,[a] Gao Hongyi,[b] Peng Xinxin,[a] Lin Min,[a] Luo Yibin,*[a] Wang Ge*[b] and Shu Xingtian[a]

The oxidative coupling of imines to ketazine with molecular oxygen is a green process towards the synthesis of hydrazine or hydrazine hydrate, which could efficiently address the economic and environmental issues of the traditional Raschig or peroxide-ketazine process. Herein, we developed an efficient heterogeneous base-free benzophenone imine oxidative coupling route with O_2 catalyzed by Cu/CuO_x/carbon materials derived from MOFs under mild conditions. Under optimized conditions, the conversion of BI is up to 98.2% and the selectivity of ketamine is 94.9%. This catalyst has excellent structure stability, recycling, and regeneration performance, owing to the carbonization of organic ligands of MOF at high temperature. More importantly, it is confirmed that the metallic Cu core is essential to improve the catalytic performance of the CuO shell in the BI oxidative coupling reaction, due to the promotion of electron transfer in the CuO surface, making dissolved O_2 molecules more easily insert oxygen vacancies. This strategy might open an avenue to the sustainable catalytic synthesis of hydrazine or hydrazine hydrate.

Received 22nd July 2020
Accepted 11th September 2020

DOI: 10.1039/d0ra06367c

rsc.li/rsc-advances

1 Introduction

The oxidative coupling of imines (especially for benzophenone imine, abbreviated as BI) provides a remarkable novel and green approach to prepare ketazines, which are the key intermediates for the synthesis of hydrazine (N_2H_4) or hydrazine hydrate ($N_2H_4 \cdot H_2O$).[1–4] N_2H_4 and $N_2H_4 \cdot H_2O$ are widely used as polymer blowing agents,[5,6] reducing reagents,[7,8] precursors of pharmaceuticals,[9,10] and high-energy fuels.[11] Traditionally, $N_2H_4 \cdot H_2O$ is majorly manufactured by the highly polluting Raschig or urea-based Raschig process (Scheme 1a).[1,12] Although H_2O_2 solution has been used as a clean oxidant to produce ketazines,[13] the peroxide-ketazine process still suffers severe economic and environmental issues, due to the high price of H_2O_2 and the generation of N-containing wastewater.[13] A fascinating alternative catalytic imine oxidative coupling route with O_2 as sole oxidant, based on Hayashi's CuCl/$ZnCl_2$ or $CuCl_2$/organic base catalytic systems, have been developed (Scheme 1b). But it is restricted by catalyst separation/recycling and alkaline waste issues.[4,14]

Recently, metal–organic frameworks (MOFs) as precursors provide a promising platform for preparing efficient carbon supported metal or metal oxide catalysts due to their high surface area, highly ordered characteristics of metal ions, tunable porosity, and multi-functionality.[15,16] Due to their advantages of excellent electron conductivity, high porosity of carbon-supported metal materials derived from MOFs, they are introduced with promising applications in batteries,[17] supercapacitors,[18,19] electrocatalytic[14] and other reactions.[20] Among of them, carbon-supported Cu materials derived from Cu-MOFs have been widely concerned, attribute to the

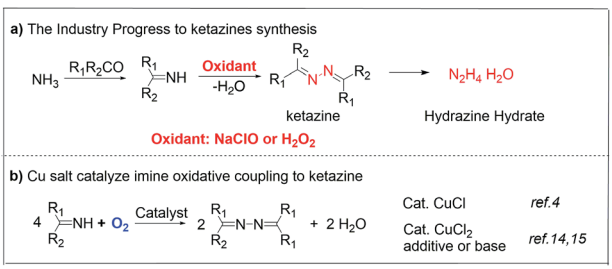

Scheme 1 Process for the production of ketazines.

[a]State Key Laboratory of Catalytic Materials and Reaction Engineering, Research Institute of Petroleum Processing, SINOPEC, 100083, Beijing, The People's Republic of China. E-mail: luoyibin.ripp@sinopec.com

[b]Beijing Advanced Innovation Center for Materials Genome Engineering, School of Materials Science and Engineering, University of Science and Technology Beijing, Beijing 100083, The People's Republic of China. E-mail: gewang33@126.com

† Electronic supplementary information (ESI) available. See DOI: 10.1039/d0ra06367c

valence changing ability between copper and its oxides, as well as the absorption and activation ability of Cu and CuO_x to H_2, O_2, CO and other small molecules. Recently, Wu group obtained a new Cu-MOF derived carbon-supported Cu/Cu_2O materials by tuning copper ligands and pyrolytic conditions, which demonstrating excellent catalytic properties in liquid-phase hydrogenation of furfural into furfuryl alcohol.[21] Lu group[22] and Chen group[23] independently found that $Cu/CuO_x/C$ materials derived from Cu–BTC can also be applied to catalyze CO oxidation reaction. $Cu/CuO_x/C$ materials with various morphologies or sizes have important influence on catalytic activity. The significant increase in electron density on the Cu/Cu_2O and Cu/CuO interface also play a pivotal role in the enhancement of CO oxidation. Although progress have been made in the field of Cu-MOFs derivatives catalysis, the types of catalytic reactions are extremely limited. In particular, there are few reports on the synthesis of organic chemicals by MOFs derivatives catalytic oxidation in liquid phase.[24,25]

Herein, to address the drawbacks in the synthesis of hydrazine hydrate, inspired by homogeneous Cu catalytic systems,[14,26] a heterogeneous Cu-MOF derived $Cu@CuO_x$ nanoparticles supported on carbon matrix ($Cu@CuO_x$/carbon) catalyst prepared *via* the direct anaerobic pyrolysis of HKUST-1 precursor in N_2 or H_2/Ar atmosphere (see Fig. 1a),[20,27–30] which exhibits excellent catalytic performance in the aerobic oxidative coupling of benzophenone imine without adding any organic base.[24,31–33] Under optimized conditions, the conversion of benzophenone imine was up to 98.2% and the selectivity of ketazine was 94.9%. More importantly, this catalyst has excellent structure stability, recycling and regeneration performance, owing to the carbonization of organic ligands of MOF at high temperature.[29,34] Consequently, this catalytic route unfolds a novel viewpoint on efficient heterogeneous preparation of ketazines, which has great industrial application potential and academic meaning.

2 Experimental

2.1 Materials

All the reagents and solvents were commercially available and used for the synthesis without further purification. Copper nitrate trihydrate ($Cu(NO_3)_2\cdot 3H_2O$, AR, Sinopharm Chemical Reagent Co., Ltd.), 1,3,5-benzenetricarboxylic acid (BTC, 98%, Aladdin), ethanol (EtOH, AR, Sinopharm Chemical Reagent Co., Ltd.), and *N*,*N*-dimethylformamide (DMF, AR, Sinopharm Chemical Reagent Co., Ltd.) were used as received.

2.2 Catalyst preparation

The HKUST precursor was prepared based on the reported literature with some modifications.[28] First, 0.48 g $Cu(NO_3)_2\cdot 3H_2O$ was added into 24 mL H_2O to prepare solution A. And 0.36 g benzene-1,3,5-tricarboxylic acid (BTC) was added into the mixture of 12 mL ethanol and 12 mL *N*,*N*-dimethylformamide to prepare solution B. Then solution A was added into solution B with stir constantly for 30 min. The mixed solution was transferred into 100 mL Teflon-lined stainless steel autoclave and heated at 85 °C for 24 h. The obtained precipitate was washed with DMF and methanol several times, then dried at 80 °C for 12 h. Then the blue HKUST-1 (Cu_3BTC_2) product was obtained.[35] 1 g HKUST was added into a crucible with a cover. The HKUST-1 was heated to the specific temperatures and kept for 2 h under N_2 or H_2/Ar atmosphere. Both the heat and cool rate was set as 5 °C min^{-1}. For example, when the catalyst is calcined in nitrogen at 400 °C for 2 hours and exposed to air at room temperature for 2 days, the obtained catalyst was labeled as $Cu@CuO_x/C–N_2$-400 + 2d.

2.3 Characterization of catalysts

X-ray photoelectron spectroscopic (XPS) experiments were carried out on a spectrometer (AXIS Supra, Kratos Analytical Ltd) with Al Kα radiation, the C 1s peak (284.6 eV) was used for the calibration of binding energy values. Scanning electron microscopy (SEM) images were taken from a Hitachi 4800 microscope (20 kV). Scanning-transmission electron microscopy (STEM) images and energy dispersive X-ray spectroscopy (EDX) of catalysts were recorded on a JEOL JEM-2100 microscope (200 kV). The samples were dispersed in anhydrous alcohol using the ultrasonic technique, the suspension obtained was added dropwise to a micro-grid membrane and dried in air. ^{1}H, ^{13}C-NMR spectra were recorded with a Varian 700 M spectrometer. Chemical shifts (in ppm) were referenced to $CDCl_3$ (δ = 7.26 ppm) or TMS (δ = 0.00 ppm) as an internal standard.

2.4 Catalytic performance tests

In a typical reaction, to a 25 mL reaction vessel, were added 50 mg catalyst and 1.0 mmol benzophenone imine in 2 mL of solvent. The heterogeneous solution was stirred at 80 °C for 24 h under 1 O_2 balloon. Imine conversion and product selectivity were analyzed by gas chromatography (GC). The product and side products were determined by GC-MS and 700 MHz ^{1}H NMR spectroscopy analysis.[36] The performance of the catalyst was evaluated by imine conversion (x), selectivity (s) and ketazine formation rate r (mmol g^{-1} h^{-1}).

Conversion (%)

$$x = (1 - n_1) \times 100\%$$

Benzophenone-azine (ketazine) selectivity (%)

$$s = (n_2/(n_2 + n_3 + n_4)) \times 100\%$$

Ketazine formation rate (mmol g^{-1} h^{-1})

$$r = 0.833sx$$

n_i is the mole fraction of component; i is 1, 2, 3 and 4, which represent the components benzophenone imine, benzophenone-azine, *N*-(2-chloroethyl)-1,1-diphenylmethylaniline and benzophenone; 0.833 = 1000 mg/(50 mg·24 h).

2.5 Recycled experiments

Catalytic stability and regeneration method: add 220 mg of $Cu@CuO_x/C–N_2$-400-20d catalyst, 6 mL of dichloromethane, and 800 mg (5 mmol) of diphenylketimine to the reaction flask

and keep the reaction temperature to 80 °C under the oxygen balloon. After 72 h, dichloromethane adds into the reaction to quench. After the catalyst was centrifuged twice, it was separated and dried at room temperature for 2 hours, followed by the next cycle experiment.

3 Results and discussion

As illustrated in Fig. 1a, three sharp diffraction peaks with 2θ peaks located at 43°, 50° and 74° in X-ray powder diffraction (XRD) spectra are observed, which are indexed to the Cu (111), (200) and (220) crystalline planes of metallic Cu (JCPDS # 04-0836), respectively.[37] It is inferred that under the effects of high temperature and reductants (such as ligand derived carbon and H_2), the aggregated Cu particles are transformed from the framework Cu sites of HKUST-1 during pyrolysis processing. Moreover, by employing Scherrer's formula, it is confirmed that the calculated aggregation degree of Cu particles is along with the increase of pyrolysis temperature, as shown in Fig. S2.† When the as-made samples exposed to air for a specific duration (the corresponding samples are referred to as Cu@CuO_x/C–400-N_2 + 2d and Cu@CuO_x/C–400-N_2 + 20d, with the exposure time of 2 days and 20 days, respectively), a significant 2θ peak at around 36.5° ascribing to Cu_2O (111) plane (JCPDS # 78-2076) formed. And the peak strength is correlated to the exposure time, suggesting the slow aerobic oxidation of metallic Cu particles by O_2 in the air.[38–40] Meanwhile, this oxidation process was directly verified by X-ray photoelectron spectroscopy (XPS). As shown in Fig. 1b, the peak intensity of CuO increases with the extension of exposure time, indicating that the surface Cu_2O (binding energy of 932.6 eV) is transformed into CuO (binding energy of 934.4 eV), which can be powerfully supported by Cu Auger spectroscopy (Cu LMM). It is demonstrated that the oxidation Cu-containing particles occur from external surface to inner core, resulting in the formation of core–shell Cu@CuO_x composite material.[37–41]

After calcination and carbonization of trimethylbenzoic acid ligand, copper aggregates to form octahedral and irregular derivative particles (Fig. 2a). Due to the large volume of octahedron, it is hard to well characterized by TEM analysis. However, the irregular shape particles were partially dissociated after the sample was pretreated with ethanol and ultrasonic treatment before TEM experiments. We were surprised to find that the irregular shaped particles were composed of copper carbon nanospheres with the size of about 40–50 nm, as shown in Fig. 2c and S3a.† The high-resolution TEM image demonstrates that Cu_2O (111) and Cu (111) located in the shell and core of Cu@CuO_x/C–400-N_2 + 20d (Fig. 2d), which is consistent with the analysis results of XRD and XPS. According to STEM-EDS mapping data, the atomic ratio of Cu, C, and O elements in the Cu@CuO_x/C–N_2-400 + 20d is 69%, 25%, and 6% (Fig. 2e and S4†). The N_2 adsorption–desorption curves (see Fig. S5†) show that the specific surface and the external surface area of the sample is 24.2 $m^2\ g^{-1}$ and 11.9 $m^2\ g^{-1}$, respectively. The average pore width of Cu@CuO_x/C–400-N_2 + 20d is up to 71.6 nm, and therefore the Cu-based active sites have good substrate accessibility.

In Table 1, benzophenone-azine **A** is the target product of the BI oxidative coupling, while two side products, benzophenone **B** and *N*-(2-chloroethyl)-1,1-diphenylmethanimine **C** are caused by the hydrolysis of BI and proposed imine *N*-alkylation with dichloroethane, respectively. Worthy to note that all the products were determined by GC-MS and ^1H, ^{13}C NMR analysis in Fig. S6.†[36] It is confirmed that **B** and **C** are two competitive products in benzophenone-azine **A** synthesis process, as shown in Table 1. It should be noted that BI is easy to hydrolyze to produce ammonia and benzophenone.[42] To restrict the hydrolysis of BI, the pH value of the mixture of BI and various solvents is set at 8.0 in our experiments (Fig. S7†). When different homogeneous Cu salt catalysts are used, the generation of Cu-imine complexes as Lewis acid may facilitate the hydrolysis of BI, with side product **B** selectivity up to 47.6% and 58.4%, respectively, as entries 1 and 2 in Table 1. In the contrary, various kinds of heterogeneous Cu@CuO_x/carbon catalysts possess more excellent benzophenone-azine **A** selectivity, higher than 85%, and up to 94.2% in maximum, as entries 3–6 in Table 1.

While under the same conditions, the selectivity of product **A** is only 3.4% for the HKUST-1 catalyst,[43] see entry 7 in Table 1. As a result, it is suggested that Cu oxides are promising active sites for the oxidative coupling reaction of BI with O_2, rather than Cu^{II} in alkaline solution or organic solvent.

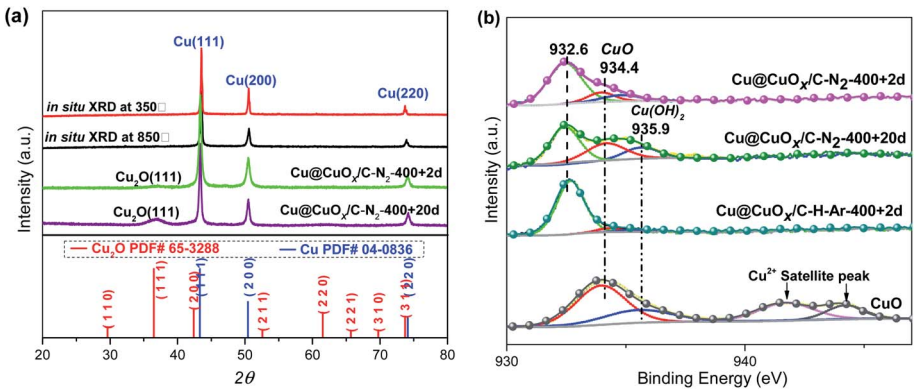

Fig. 1 (a) XRD and *in situ* XRD patterns of HKUST-1 derivatives; (b) XPS spectrums of HKUST-1 derivatives and CuO.

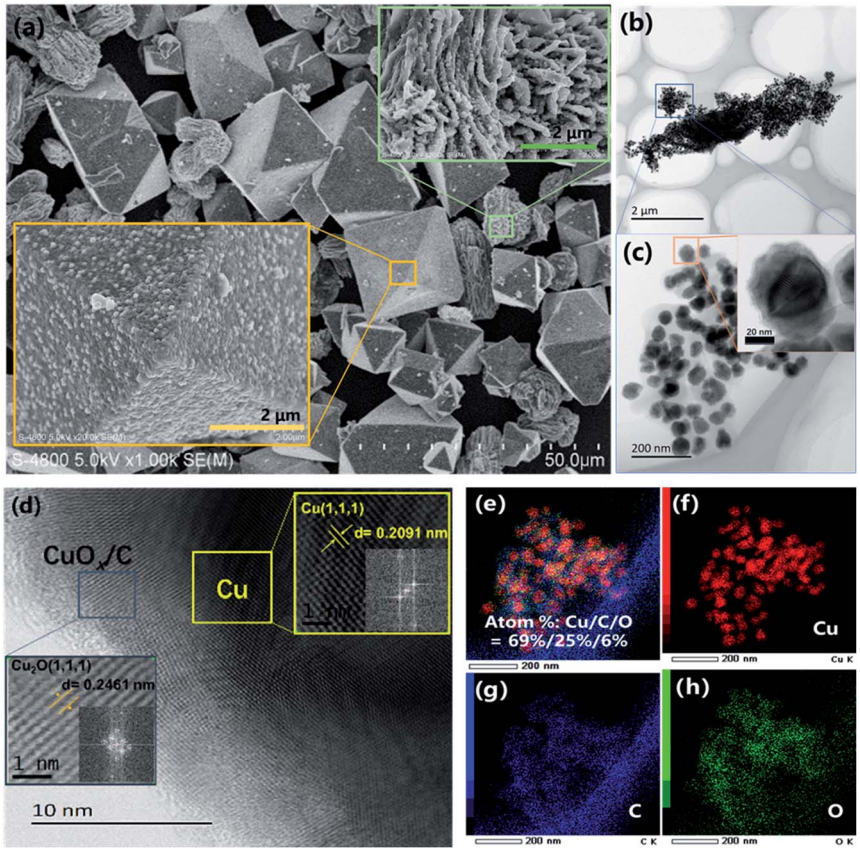

Fig. 2 (a) SEM analysis of Cu@CuO_x/C–N_2-400 + 20d material; (b–d) HR-TEM spectrum of Cu@CuO_x/C–N_2-400 + 20d; (e–h) STEM-EDS mapping images of Cu@CuO_x/C–N_2-400 + 20d.

Moreover, core–shell Cu@CuO_x/carbon catalysts generally perform higher BI conversion and better selectivity than commercial CuO and Cu_2O powders. More in detail, Cu@CuO_x/C–N_2-400 + 2d as a catalyst, the 83.5% BI conversion, and the 94.0% product **A** selectivity, which is much higher than that of CuO powder (38.1% BI conversion, 86.3% product **A** selectivity), as shown in entries 8 and 9, Table 1. It is reasonably attributed to the smaller particle size and unique induced effect of Cu core on CuO_x shell,[44] which is conducive to the adsorption of BI and the H abstraction by Lewis acid site to promote the imine dehydration oxidative coupling reaction. Moreover, it is found that increasing the exposure time and pyrolysis temperature (corresponding to Cu@CuO_x/C–N_2-400 + 20d and Cu@CuO_x/C–N_2-850 + 20d, respectively) have a slight negative impact on BI conversion. While the selectivity was maintained at 94%, the BI conversion decreased by 5.8% and 8.3%, respectively. When using H_2 as reductant, the Cu@CuO_x/C–H–Ar-400 + 2d shows even higher BI conversion (reaching 87.7%), but the selectivity of product **A** drops to 91.4%. Consequently, by combining with characterization results, it confirms that higher Cu and Cu_2O content is in favor of more promising catalytic performance in oxidative coupling reaction, which may be accelerated by oxygen radical species and lattice oxygen species in principle. Therefore, in order to ruling out possible oxygen radical species, several free radical scavengers were added to the general reaction process, and without significant impact on the catalytic performance Cu@CuO_x/C–N_2-400 + 20d, as shown in Table S1,† indicating that lattice oxygen species involved in the oxidative reaction.[45]

Interestingly, owing to the difference of solubility between organic solvents and water, chlorinated solvents, *e.g.*, dichloroethane, trichloromethane and 1-chloropropane, perform remarkably enhanced both BI conversion and **A** selectivity than those of other chloride-free solvents, *e.g.*, acetonitrile and dioxane, as shown in entries 10–13 in Table 1. In more detail, BI and product **A** completely dissolve in hydrophobic chlorinated solvents to preventing BI hydrolysis, while acetonitrile and dioxane can make organic subtracts/products and water homogeneously dissolved. More than that, probably due to the number and position of chlorine atoms in these two solvents decrease the activity of alkylation reaction, when chloroform or 1-chloropropane was used as solvents, no corresponding *N*-alkylation of imines was detected by GC or GC-MS (Fig. S8†). The influence of halogen-containing solvents on this oxidative coupling reaction needs to be further explored and summarized, which will be further explained in the follow-up research.

The catalytic performance of Cu@CuO_x/C–N_2-400 + 20d becomes gradually decreased along with the increasing of recycle times, with BI conversion and ketazine selectivity reducing from 94.5% and 87% at initial stage to 46.2% and

Table 1 Catalyst screening and reaction condition optimization for oxidative coupling of benzophenone imine[a]

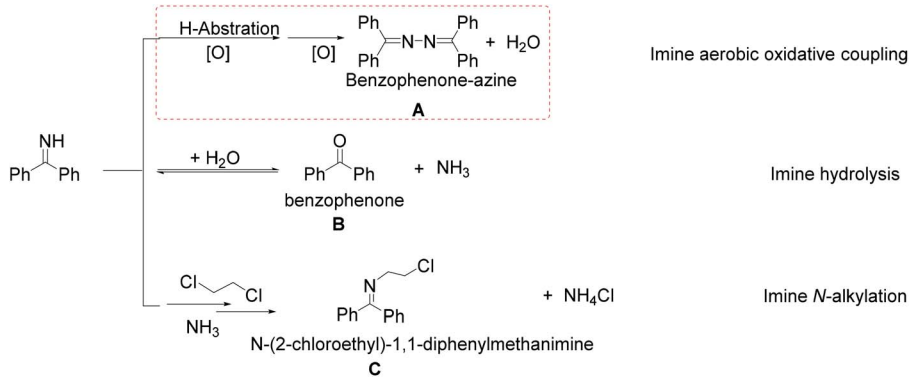

Entry	Catalyst	Solvent[e]	Conversion (%)	Selectivity (%)		
				A	B	C
1[b]	$Cu(OAc)_2 \cdot H_2O$	1,2-Dichloroethane	97.5	51.2	47.6	1.2
2[b]	$CuCl_2 \cdot 2H_2O$	1,2-Dichloroethane	96.4	40.7	58.4	0.8
3	$Cu@CuO_x/C–N_2$-400 + 2d	1,2-Dichloroethane	83.5	94.0	4.9	1.1
4	$Cu@CuO_x/C–N_2$-400 + 20d	1,2-Dichloroethane	77.7	94.1	4.6	1.3
5	$Cu@CuO_x/C–N_2$-850 + 20d	1,2-Dichloroethane	75.2	94.2	4.6	1.2
6	$Cu@CuO_x/C–H–Ar$-400 + 2d	1,2-Dichloroethane	87.7	91.4	6.3	2.3
7	HKUST-1	1,2-Dichloroethane	30.1	3.4	75.4	21.2
8[c]	CuO	1,2-Dichloroethane	38.1	86.3	7.5	6.2
9[c]	Cu_2O	1,2-Dichloroethane	46.2	90.5	4.8	4.7
10[d]	$Cu@CuO_x/C–N_2$-400 + 20d	Trichloromethane	95.0	86.0	14.0	0
11[e]	$Cu@CuO_x/C–N_2$-400 + 20d	1-Chloropropane	91.0	94.8	5.2	0
12	$Cu@CuO_x/C–N_2$-400 + 20d	Acetonitrile	27.5	42.3	57.7	0
13	$Cu@CuO_x/C–N_2$-400 + 20d	1,4-Dioxane	42.9	30.7	69.3	0

[a] Reaction conditions: 2 mL solvent, 50 mg HKUST-1 or HKUST-1 derived catalyst, 1 mmol BI, 80 °C, 24 h, 1 O_2 balloon. Yields are determined by GC spectroscopy. All the product and by-products were determined by ^1H, ^{13}C NMR and GC-MS, see ESI for more information. [b] 20% mmol metal salts as the catalyst. [c] 1 mmol Cu catalyst. [d] No corresponding imine alkylation product was detected. [e] No corresponding imine alkylation products were detected.

76.5% after six recycles, respectively (Fig. 3). Corresponding, in accordance with XRD analysis, deactivated catalyst possesses crystalline CuO phases with (110), (−111), (111) and (−202) planes (JCPDS # 80-1916), corresponding to 2θ of 32.5°, 35.6°, 38.8°, and 48.9° (blue line in Fig. 4a). Meanwhile, it can be seen from the Cu $2p_{3/2}$ XPS spectrum that the surface Cu species of the deactivated catalyst mainly exists in the form of CuO. The peak with binding energy of 934.4 eV and satellite peak are almost the same as that of commercial CuO powder, indicating that Cu and Cu_2O of $Cu@CuO_x/C–N_2$-400 + 20d are completely oxidized to CuO (Fig. 4b).[46] To recover the initial catalytic activity, the deactivated catalyst was regenerated by H_2/Ar (5%/95%) gas mixtures at 400 °C for 1 hour. Interestingly, the BI conversion and ketazine selectivity of regenerated catalyst is up to 98.2% and 94.9%, respectively, even higher than those of fresh $Cu@CuO_x/C–N_2$-400 + 2d catalyst. In Fig. 4a, three sharp diffraction peaks of metallic Cu (JCPDS # 04-0836) were detected in the XRD patterns of regenerated catalyst (red line), suggesting that CuO can be quickly reduced to Cu_2O and metallic Cu by H_2/Ar atmosphere at high temperature through a facial reduction method.[47,48] This transformation was further confirmed by the appearance of the peak at 932.6 eV in Cu $2p_{3/2}$ XPS (Fig. 4b). In addition, from SEM images of deactivated catalyst (Fig. S9†), the morphology and size of nanoparticles are well maintained.

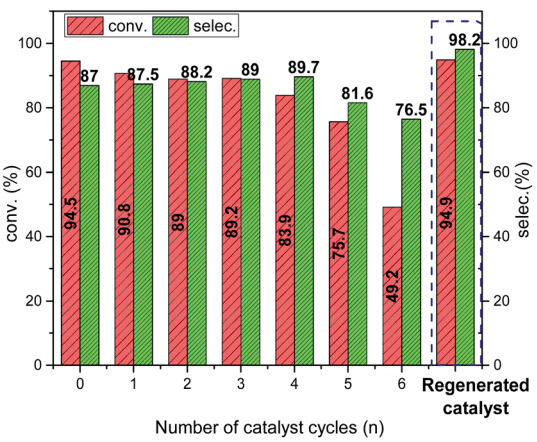

Fig. 3 Recycling experiments by the catalysis of $Cu@CuO_x/C–N_2$-400 + 20d.

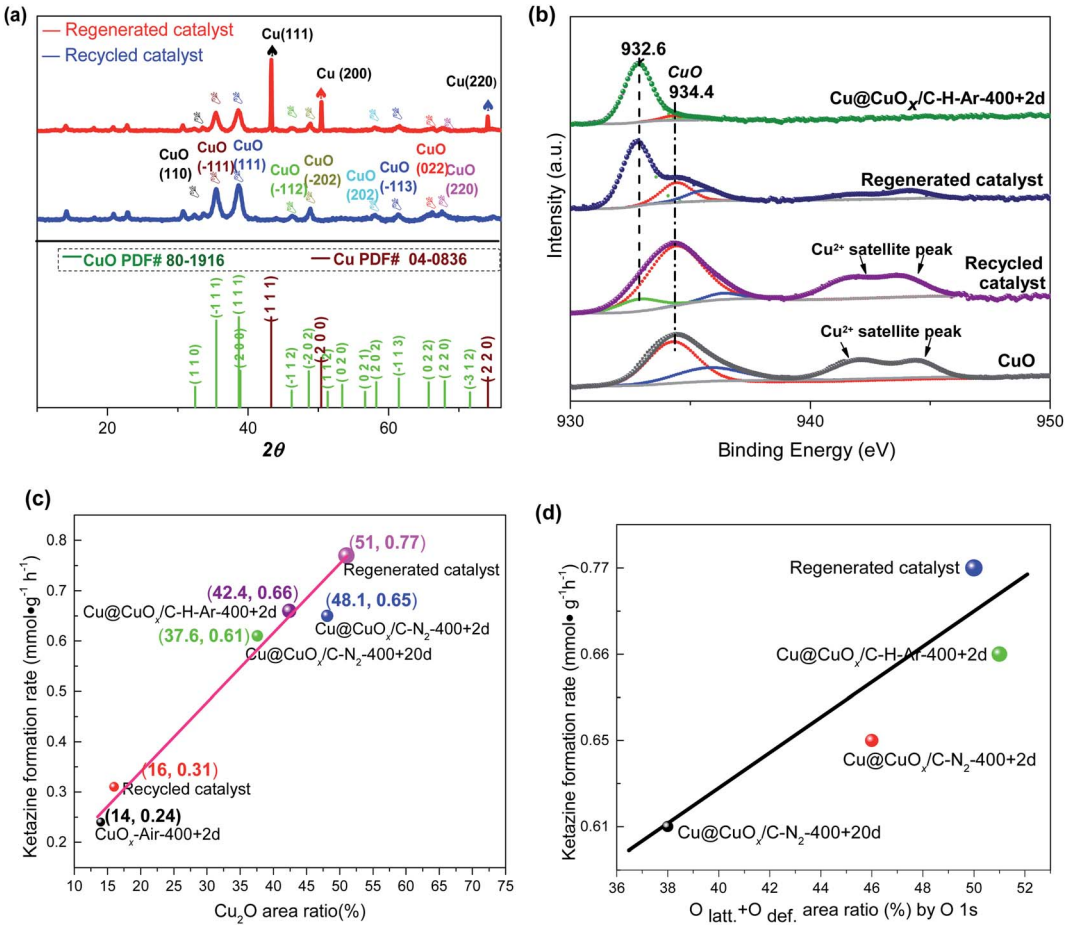

Fig. 4 (a and b) XRD pattern and XPS analysis of regenerated and recycled catalyst; (c) correlation between Cu_2O ratio and ketazine formation rates; (d) correlation between the total area of lattice oxygen plus defect oxygen and ketazine formation rates.

However, the original octahedral carbon matrix becomes irregular. Nevertheless, ICP-OES analysis demonstrates that the Cu leaching is negligible after several recycles, therefore showing its excellent application potential (Fig. S10†). Totally, it strongly infers that significant increase in the density of low-valence Cu species (including metallic Cu and Cu_2O) favors the enhanced catalytic performance for BI oxidative coupling reaction, as shown in Fig. 2d and S11.† Specifically, when the Cu_2O area ratio rises from 14% to 50%, the ketazine formation rate increased linearly from 0.24 mmol g^{-1} h^{-1} to 0.77 mmol g^{-1} h^{-1}, which suggests that Cu_2O and metallic Cu species have induction effects on CuO and then facilitate the generation and transformation of active oxygen species.[49–51] Furthermore, the O 1s XPS spectra directly proved that the high content of lattice oxygen and defect oxygen in the catalyst was beneficial to the high yield of ketazine (see Fig. 4d and S12†). Owing to the enhancement of electron transfer on CuO surface induced by low valence Cu and Cu_2O core, which makes the formation and donation of lattice oxygen much more accessible.[52] Once the metal Cu is finally oxidized to CuO, the promoting electron effect would be weakened, and its catalytic performance is similar to that of commercial CuO powder.

On the basis of the study of surface composition and the corresponding catalytic activities, a synergetic catalytic mechanism was proposed where O_2 molecules adsorbed on Cu_2O to form Cu(II)–O_2–Cu(II) intermediate, and then the oxygen activated by copper split into oxygen adatoms and transfer to fill the oxygen vacancies on CuO.[53] Imine adsorbed on CuO is oxidatized dehydrogenation into Cu-imine species by the lattice oxygen of CuO. It is suggested that two redox semi-reactions involved in the heterogeneous BI oxidative coupling: (1) oxidative BI coupling by the active oxygen species of CuO, with the formation of ketazine (containing N–N bonds), water and Cu_2O; (2) the aerobic oxidation of Cu_2O to CuO, making oxygen adatoms insert the oxygen vacancy sites, as illustrated in Scheme 2.[26] In a general procedure, the surface Cu^{II} species acted as Lewis acid sites make the H–N bonds of BI more active, through the charge transfer between Cu sites and N atoms in imine groups. Then, the activated H atom is oxidized by the surface lattice oxygen species to produce water and oxygen vacancies, and the divalent copper is reduced to monovalent copper; in the meantime, the N–N bond is oxidized to ketazine. After that, Cu_2O is re-oxidized by O_2 to CuO, with the finishing of one catalytic recycle. The Lewis acidity and redox capacity of Cu-containing sites are

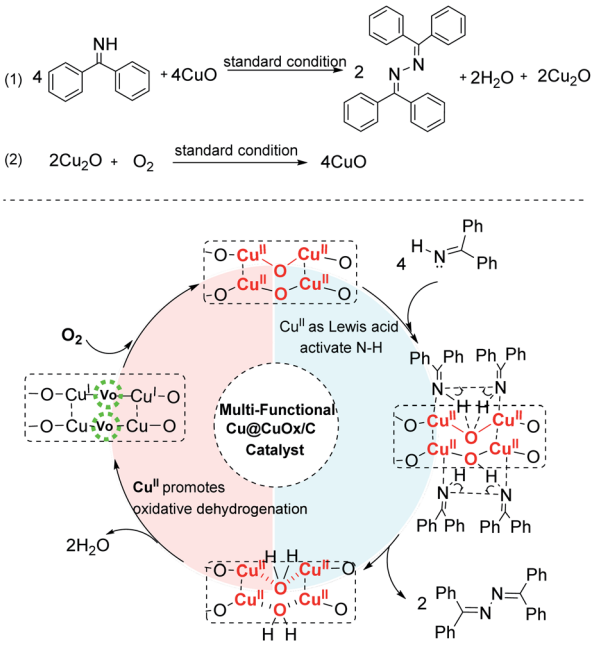

Scheme 2 Plausible catalytic mechanism.

apparently synergistical to boost both BI activation and active oxygen species transfer, thus exhibiting excellent BI conversion and ketazine selectivity.

4 Conclusions

In summary, a novel and efficient heterogeneous oxidative BI coupling route catalyzed by Cu@CuO_x/carbon composites without the assistance of organic base, has been developed. Under the optimized conditions, the Cu@CuO_x/carbon catalyst not only offers 98.2% BI conversion and 94.9% ketazine selectivity, but also possess exciting regeneration ability. More importantly, it is suggested that the metallic Cu core is essential to improve the catalytic performance of CuO shell in BI oxidative coupling reaction, because it promotes the electron transfer on CuO surface and makes the dissolved O_2 molecules more easily inserted into the oxygen vacancies. The enhanced redox cycle between Cu^I and Cu^{II} plays an essential role in BI activation, the dehydrated coupling of BI and the regeneration of active sites. Therefore, the low-valence Cu content is closely relevant with BI conversion and ketazine selectivity. With the increase of catalyst recycling times, Cu@CuO_x/carbon catalyst was slowly deactivated but could be entirely regenerated by a facial hydrogenation process. Hence, this heterogeneous oxidative coupling method has ultra-important potential for sustainable catalytic synthesis of hydrazine hydrate.

Conflicts of interest

There are no conflicts to declare.

Notes and references

1 H. Hayashi, *Catal. Rev.*, 1990, **32**, 229–277.
2 E. W. Schmidt, in *Hydrazine and Its Derivatives: Preparation, Properties, Applications*, Wiley-Blackwell, New York, 2001, p. 2122.
3 E. Rothgery, in *Hydrazine and Its Derivatives*, 2004, vol. 13.
4 H. Hayashi, A. Kainoh, M. Katayama, K. Kawasaki and T. Okazaki, *Prod. R&D*, 1976, **15**, 299–303.
5 A. S. Dutta, in *Recycling of Polyurethane Foams*, ed. S. Thomas, A. V. Rane, K. Kanny, V. K. Abitha and M. G. Thomas, William Andrew Publishing, 2018, pp. 17–27.
6 G. Wypych, in *Handbook of Foaming and Blowing Agents*, ed. G. Wypych, ChemTec Publishing, 2017, pp. 123–177.
7 A. Furst, R. C. Berlo and S. Hooton, *Chem. Rev.*, 1965, **65**, 51–68.
8 D. Formenti, F. Ferretti, F. K. Scharnagl and M. Beller, *Chem. Rev.*, 2019, **119**, 2611–2680.
9 C. H. Zhou and Y. Wang, *Curr. Med. Chem.*, 2012, **19**, 239–280.
10 J. P. Schirmann and P. Bourdauducq, *Hydrazine*, Wiley-VCH Verlag GmbH & Co. KGaA, 2001.
11 G. D. Byrkit and G. A. Michalek, *Ind. Eng. Chem. Res.*, 1950, **42**, 1862–1875.
12 F. Raschig, *Ber. Dtsch. Chem. Ges.*, 1907, **40**, 4580–4588.
13 P. Nikhitha and K. B. S. Saibabu, *Chem. Eng. Technol.*, 2010, **33**, 1543–1551.
14 A. Laouiti, M. M. Rammah, M. B. Rammah, J. Marrot, F. Couty and G. Evano, *Org. Lett.*, 2012, **14**, 6–9.
15 W. Yang, X. Li, Y. Li, R. Zhu and H. Pang, *Adv. Mater.*, 2019, **31**, 1804740.
16 W. Chaikittisilp, K. Ariga and Y. Yamauchi, *J. Mater. Chem. A*, 2013, **1**, 14–19.
17 X. Zhang, A. Chen, M. Zhong, Z. Zhang and X. H. Bu, *Electrochem. Energy Rev.*, 2019, **2**, 29–104.
18 R. R. Salunkhe, Y. V. Kaneti, K. Jeonghun, J. Ho and Y. Yamauchi, *Acc. Chem. Res.*, 2016, **49**, 2796–2806.
19 J. Wang, M. Rao, C. Ye, Y. Qiu, W. Su, S. R. Zheng, J. Fan, S. L. Cai and W. G. Zhang, *RSC Adv.*, 2020, **10**, 4621–4629.
20 K. Shen, X. Chen, J. Chen and Y. Li, *ACS Catal.*, 2016, **6**, 5887–5903.
21 K. Chen, J. L. Ling and C. D. Wu, *Angew. Chem.*, 2020, **59**, 1925–1931.
22 S. Zhang, H. Liu, C. Sun, P. Liu, L. Li, Z. Yang, X. Feng, F. Huo and X. Lu, *J. Mater. Chem. A*, 2015, **3**, 5294–5298.
23 R. Zhang, L. Hu, S. Bao, R. Li, L. Gao, R. Li and Q. Chen, *J. Mater. Chem. A*, 2016, **4**, 8412–8420.
24 C. Bai, A. Li, X. Yao, H. Liu and Y. Li, *Green Chem.*, 2016, **18**, 1061–1069.
25 R. Fang, R. Luque and Y. Li, *Green Chem.*, 2016, **18**, 3152–3157.
26 M. C. Ryan, Y. J. Kim, J. B. Gerken, F. Wang, M. M. Aristov, J. R. Martinelli and S. S. Stahl, *Chem. Sci.*, 2020, **11**, 1170–1175.
27 D. Farrusseng, S. Aguado and C. Pinel, *Angew. Chem., Int. Ed.*, 2009, **48**, 7502–7513.
28 H. C. Zhou and S. Kitagawa, *Chem. Soc. Rev.*, 2014, **43**, 5415–5418.
29 A. Corma, H. Garcia and F. X. Llabres i Xamena, *Chem. Rev.*, 2010, **110**, 4606–4655.

30 P. A. Julien, C. Mottillo and T. Friščić, *Green Chem.*, 2017, **19**, 2729–2747.
31 X. Zhang, W. Dong, Y. Luan, M. Yang, L. Tan, Y. Guo, H. Gao, Y. Tang, R. Dang, J. Li and G. Wang, *J. Mater. Chem. A*, 2015, **3**, 4266–4273.
32 Y. Luan, Y. Qi, H. Gao, R. S. Andriamitantsoa, N. Zheng and G. Wang, *J. Mater. Chem. A*, 2015, **3**, 17320–17331.
33 W. Zhong, H. Liu, C. Bai, S. Liao and Y. Li, *ACS Catal.*, 2015, **5**, 1850–1856.
34 A. Dhakshinamoorthy, A. M. Asiri and H. Garcia, *Chem. Commun.*, 2014, **50**, 12800–12814.
35 K. Schlichte, T. Kratzke and S. Kaskel, *Microporous Mesoporous Mater.*, 2004, **73**, 81–88.
36 K. Li, X. Shao, L. Tseng and S. J. Malcolmson, *J. Am. Chem. Soc.*, 2018, **140**, 598–601.
37 Y. J. Chen, M. H. Li, J. C. Huang and P. Chen, *Sci. Rep.*, 2018, **8**, 7646.
38 Q. Zhu, L. Zou, G. Zhou, W. A. Saidi and J. C. Yang, *Surf. Sci.*, 2016, **652**, 98–113.
39 I. Platzman, R. Brener, H. Haick and R. Tannenbaum, *J. Phys. Chem. C*, 2008, **112**, 1101–1108.
40 Z.-J. Zuo, J. Li, P.-D. Han and W. Huang, *J. Phys. Chem. C*, 2014, **118**, 20332–20345.
41 M. C. Biesinger, *Surf. Interface Anal.*, 2017, **49**, 1325–1334.
42 R. W. Layer, *Chem. Rev.*, 1963, **63**, 489–510.
43 L. Mitchell, B. Gonzalez-Santiago, J. P. S. Mowat, M. E. Gunn, P. Williamson, N. Acerbi, M. L. Clarke and P. A. Wright, *Catal. Sci. Technol.*, 2013, **3**, 606–617.
44 C. Sarkar, S. Pendem, A. Shrotri, D. Q. Dao, P. Pham Thi Mai, T. Nguyen Ngoc, D. R. Chandaka, T. V. Rao, Q. T. Trinh, M. P. Sherburne and J. Mondal, *ACS Appl. Mater. Interfaces*, 2019, **11**, 11722–11735.
45 J. J. Varghese, Q. T. Trinh and S. H. Mushrif, *Catal. Sci. Technol.*, 2016, **6**, 3984–3996.
46 R. P. Vasquez, *Surf. Sci. Spectra*, 1998, **5**, 262–266.
47 S. D. Pike, E. R. White, A. Regoutz, N. Sammy, D. J. Payne, C. K. Williams and M. S. Shaffer, *ACS Nano*, 2017, **11**, 2714–2723.
48 A. P. LaGrow, M. R. Ward, D. C. Lloyd, P. L. Gai and E. D. Boyes, *J. Am. Chem. Soc.*, 2017, **139**, 179–185.
49 S. Yadav, A. Jain and P. Malhotra, *Green Chem.*, 2019, **21**, 937–955.
50 T.-J. Huang, *Catal. Lett.*, 2003, **87**, 173–178.
51 L. Wan, Q. Zhou, X. Wang, T. E. Wood, L. Wang, P. N. Duchesne, J. Guo, X. Yan, M. Xia, Y. F. Li, A. A. Jelle, U. Ulmer, J. Jia, T. Li, W. Sun and G. A. Ozin, *Nat. Catal.*, 2019, **2**, 889–898.
52 T. Kangas, K. Laasonen, A. Puisto, H. Pitkänen and M. Alatalo, *Surf. Sci.*, 2005, **584**, 62–69.
53 B. Wei, N. Yang, F. Pang and J. Ge, *J. Phys. Chem. C*, 2018, **122**, 19524–19531.